Short nanometer range optically induced magnetic fluctuations accompanying ultrafast demagnetization of nanoscale ferromagnetic domains

Sergey Suturin, Andre Philippi-Kobs, Robert Carley, Rafael Gort, Gerhard Grübel, Emmanuelle Jal, Marina Baidakova, Eugeniya Yu. Lobanova, Laurent Mercadier, Serguei Molodtsov, et al.

Short nanometer range optically induced magnetic fluctuations accompanying ultrafast demagnetization of nanoscale ferromagnetic domains

Sergey M. Suturin,[1,*] Andre Philippi-Kobs,[2] Robert Carley,[3] Rafael Gort,[3] Gerhard Grübel,[2,3] Emmanuelle Jal,[4] Marina V. Baidakova,[1] Eugeniya Yu. Lobanova,[5] Laurent Mercadier,[3] Serguei L. Molodtsov,[3,6] Leonard Müller,[7] Dmitrii V. Potorochin,[2,3,6] Matthias Riepp,[2] Wojciech Roseker,[2] Andreas Scherz,[3] Justine Schlappa,[3] Loïc Le Guyader,[3] Giuseppe Mercurio,[3] Monica Turcato,[3] Benjamin Van Kuiken,[3] Alexander Yaroslavtsev,[2,8] Alexander Y. Deviatov,[9] Yaroslav O. Kvashnin,[8] Alexander I. Lichtenstein,[10] Vladimir V. Mazurenko,[9] and Igor I. Pronin[1,5]

[1]*Ioffe Institute, 26 Polytechnicheskaya, 194021 Saint Petersburg, Russia*
[2]*Deutsches Elektronen-Synchrotron DESY, Notkestrasse 85, D-22607 Hamburg, Germany*
[3]*European XFEL, Holzkoppel 4, D-22869 Schenefeld, Germany*
[4]*Sorbonne Université, CNRS, Laboratoire de Chimie Physique—Matière et Rayonnement, LCPMR, 75005 Paris, France*
[5]*ITMO University, Kronverksky prospekt 49, 197101 Saint Petersburg, Russia*
[6]*Institute of Experimental Physics, TU Bergakademie Freiberg, Leipziger Straße 23, D-09599 Freiberg, Germany*
[7]*University of Hamburg, Mittelweg 177, 20148 Hamburg, Germany*
[8]*Department of Physics and Astronomy, Uppsala University, 75120 Box 516 Sweden*
[9]*Theoretical Physics and Applied Mathematics Department, Ural Federal University, Mira Street 19, Ekaterinburg 620002, Russia*
[10]*Institute of Theoretical Physics, Department of Physics, University of Hamburg, Notkestraße 9–11, 22607 Hamburg, Germany*

(Received 13 September 2023; accepted 15 November 2023; published 29 November 2023)

We have studied the nature of optically induced short-range magnetic fluctuations occurring at 10-nm length scale during ultrafast demagnetization in ferromagnetic Co/Pt multilayers. The time resolved probing of magnetization dynamics was performed with femtosecond soft x-ray pulses at the European x-ray free-electron laser. A transient high-q magnetic scattering accompanying and directly correlated to the destruction of the maze domain network has been observed at picosecond time scale in the wave vector region of 0.2–0.8 nm^{-1}. This high-q scattering has a purely magnetic nature and is ascribed to the optically induced short-range magnetic fluctuations developing in the disturbed but not fully destroyed magnetic domain network. Finally, we have simulated the optically induced response of the domain system using a two-temperature atomistic spin model and have concluded that the reason behind the high-q scattering is the laser-driven heating inducing thermal fluctuations of the domain magnetic structure.

DOI: 10.1103/PhysRevB.108.174444

I. INTRODUCTION

The optical manipulation of the magnetization on sub-picosecond timescales has been a field of intense research since the discovery of ultrafast demagnetization in 1996 [1–3]. While the origin of ultrafast demagnetization was intensively investigated over the last decades, information of the ultrafast spatial evolution of the magnetization is scarce [4–6]. Pfau *et al.* provided the first evidence that lateral superdiffusive currents [7,8] contribute to the demagnetization of the domain network leading to a transient broadening of magnetic domain walls. The conclusion was drawn indirectly from a shift in the magnetic scattering peak related to the domain pattern. Since a direct access to sub-100-nm length scales is not given at ultraviolet free-electron laser (FEL) wavelengths, an investigation of local inhomogeneities in the magnetization dynamics was not possible in this experiment. The x-ray FEL (XFEL) study directly investigating the magnetic response upon IR pumping on a sub-100-nm-length scale was published, dealing with ferrimagnets exhibiting a single-domain state that were optically driven close to or through the ferrimagnetic-to-paramagnetic phase transition [9]. The appearance of a high-q diffraction ring with a diameter that transiently changes on a-few-picosecond time scale was attributed to dynamically varying short-range magnetic inhomogeneities caused by nonlinear magnon localization and coalescence processes [5]. For nanoscale ferromagnetic domain networks, it is still an open question whether local inhomogeneities on a 10–100 nm length scale play a crucial role in the demagnetization and remagnetization dynamics [10–12].

Here we report on IR-pump / soft-x-ray-probe investigation of the magnetization dynamics in nanoscale ferromagnetic maze-domain networks of Co/Pt multilayers with perpendicular magnetic anisotropy [6,13]. The experiment was performed at the SCS beamline of European XFEL [Fig. 1(a)] [14]. The ultrashort soft x-ray light pulses fed from XFEL at MHz-repetition rate [Fig. 1(b)] were used to take instant snapshots of spatial magnetization distribution employing resonant magnetic small-angle x-ray scattering (mSAXS) as a probe. In the present work we have detected an optically induced transient magnetic scattering signal on picosecond

*Corresponding author: suturin@mail.ioffe.ru

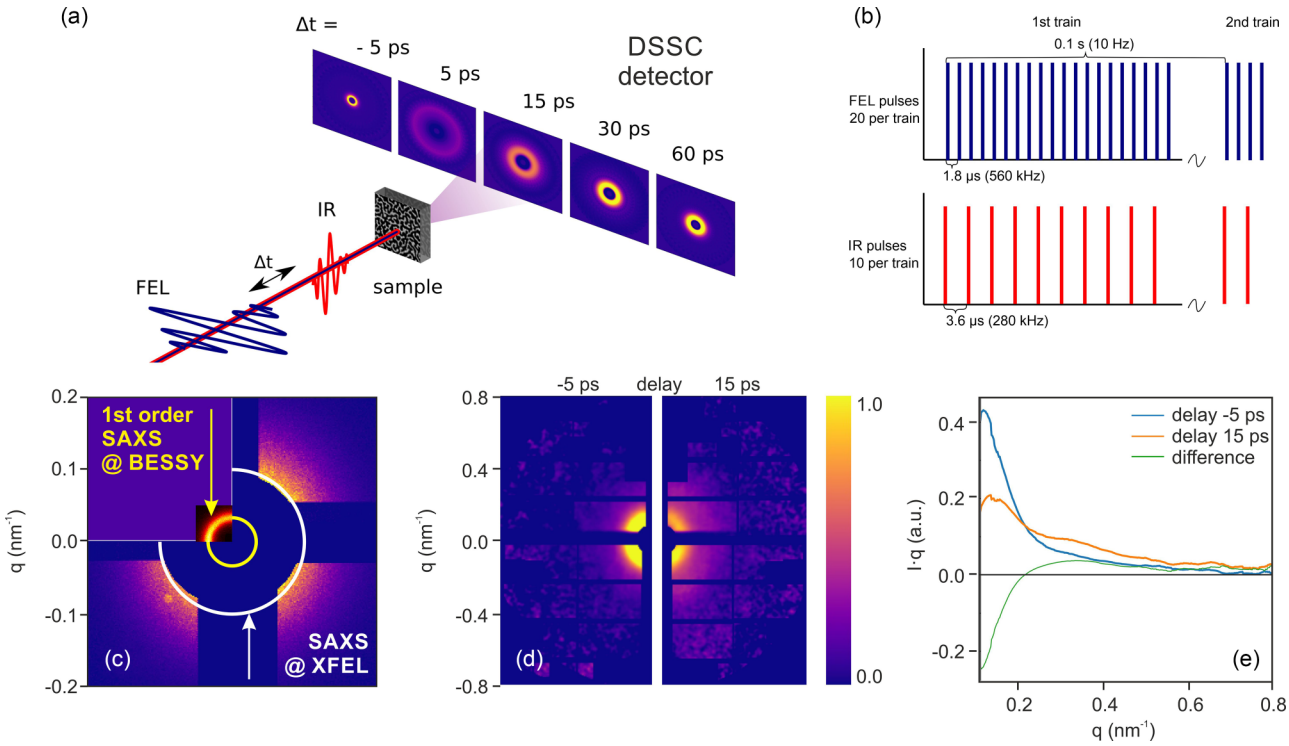

FIG. 1. mSAXS experiment and data analysis. (a) The magnetic multilayer with a magnetic maze-domain pattern is pumped by a IR-laser and probed by a FEL-pulse at time delay Δt. The resulting mSAXS signal is detected by the DSSC detector on a single-shot basis. (b) IR and FEL-pulse structure. One pulse train consists of 10 IR (20 FEL) pulses delivered with a repetition rate of 280 kHz (560 kHz); the train frequency is 10 Hz. (c) Low-q sector of the DSSC-detector signal showing the position of the third-order magnetic scattering (white ring), corresponding to the Fourier transform of sharp domain wall boundaries. The first-order magnetic scattering ring is hidden behind the beam stop. The first quadrant shows the respective first-order magnetic scattering signal of the same sample obtained at VEKMAG@BESSY II (yellow ring) [15]. (d) DSSC-detector signal for a time delay of $\Delta t = -5$ ps (left) and $\Delta t = +15$ ps (right). (e) Radial intensity I times scattering vector q vs q behavior obtained from azimuthal averaging the intensity I of the scattering images shown in (d) (blue, orange). The green curve displays the difference between both $I \cdot q(q)$ curves.

timescales in the wave-vector region above $0.2\,\mathrm{nm}^{-1}$ corresponding to lateral periodicities below 30 nm [Figs. 1(d) and 1(e)], i.e., significantly smaller than the 190-nm periodicity of the static magnetic domain pattern [Fig. 1(c)]. Based on the detailed investigation of the scattering signal as a function of IR fluence and applied magnetic field, we show that the additional transient signal appears mainly in the ferromagnetic region of the phase diagram far below IR fluences that trigger a ferromagnetic-to-paramagnetic phase transition. Moreover, in contrast to Iacocca *et al.* [9], we reveal that the high-q scattering is related to the collective excitations within the domain network, namely to the short-range fluctuations of the magnetic domain pattern upon IR excitation. The experimentally observed time evolution of the magnetic scattering has been well reproduced by a phenomenological two-temperature model simulating the spin dynamics triggered by the IR laser pulse.

II. EXPERIMENTAL

As a sample system, a Co/Pt multilayer with perpendicular magnetic anisotropy grown by sputtering techniques on 50-nm-thick Si_3N_4 membranes with lateral dimensions of $100 \times 100\,\mu\mathrm{m}^2$ was used [7]. The thicknesses of the individual Co and Pt layers were 1.0 and 1.2 nm, respectively, and a total of six repetitions of the Co and Pt was deposited on a Pt seed layer of 5 nm thickness, i.e., Pt 5.0 nm/ [Co 1.0 nm/Pt 1.2 nm]$_6$/ Pt 0.8 nm. The Pt cap layer is 2-nm-thick to prevent oxidation. After growth, the sample was demagnetized in an out-of-plane magnetic field to generate a labyrinth-like close-to-equilibrium domain state with an average lateral domain size of ≈95 nm. The domains are topologically congruent in the perpendicular direction. A chip with a total of 64 membranes (array of 8 × 8 with a pitch in both directions of 1 mm) was used for the experiment.

The experiment was conducted using a pump-probe scheme with x-ray FEL probe radiation resonantly tuned to the L_3 edge of Co ($E_{\mathrm{ph}} = 778$ eV). The FEL was operated at 560 kHz delivering 20 probe-pulses per train with 10 trains per s [Fig. 1(b)]. The duration of each x-ray light pulse was 25 fs. The IR pump laser ($\lambda = 800$ nm) was synchronized to the FEL pulses so that a variable delay time Δt between the pump and the probe could be set. The data was collected in runs consisting around 10000 trains with the delay time either fixed to a constant value or scanned back and forth between −5 ps and +60 ps. The mSAXS patterns were collected in transmission geometry on a single-shot basis using the DSSC (depleted field effect transistor sensor with signal compression) detector [16] positioned at 600-mm downstream of the sample. The angular size of the DSSC detector used in

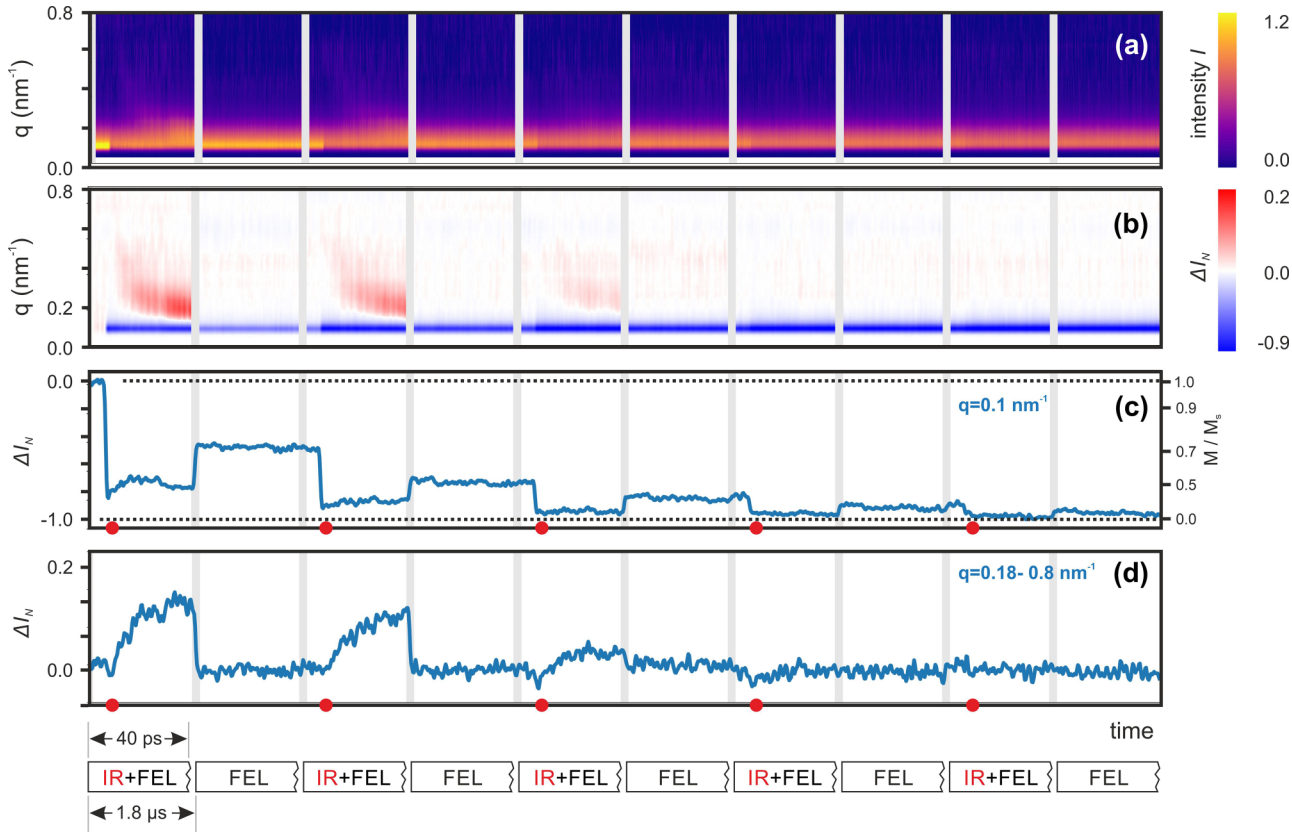

FIG. 2. Temporal evolution of the scattering intensity for the first ten FEL pulses in a train ($n \leqslant 10$) for a fluence of $f = 5.6$ mJ/cm². The maximum time delay per n is 40 ps; the FEL pulses in a train are separated by 1.8 μs. Only for odd n the sample is pumped by the IR pulse. (a) Azimuthally averaged detector signal I vs scattering vector q, time delay Δt, and n. (b) Normalized differential signal ΔI_N obtained from (a) particularly revealing a transient scattering signal in the high-q region for $n = 1,\ 3,\ 5$. (c) and (d) display the temporal evolution of ΔI_N for $q = 0.1$ nm^{-1} and $q \in (0.18{-}0.8$ nm$^{-1})$, respectively. The square root of $\Delta I_N(q = 0.1$ nm$^{-1})$ serves as a measure for the saturation magnetization M_S.

the XFEL experiment was about 20 times larger compared to the diameter of the first-order scattering ring from the maze domains [Fig. 1(c)]. For technical reasons the first-order scattering ring was hidden behind the beam stop located in the central part of the detector and could not be observed. With the second-order scattering ring forbidden for the square meander lateral magnetization distribution, the only scattering from magnetic domains observed in the present experiment was the third-order scattering ring [Fig. 1(c)]. Compared to the FEL, the IR laser was operated at a twice smaller frequency of 280 kHz delivering 10 pump-pulses per train, such that every odd-numbered FEL pulse probed the pumped state on a picosecond time scale while every even-numbered FEL pulse probed the pumped state about 1.8 μs after the arrival of the latest IR pulse. The timing of the pump-probe method employed was initially chosen assuming that the sample fully recovers within 3.6 microseconds from one IR pulse to the next. As will be discussed later in the text, this condition was not fulfilled. Thus, only the first IR pulse in the train interacted with the magnetic system in an equilibrium.

III. RESULTS

The typical mSAXS patterns obtained 5 ps before and 15 ps after the IR pulse are shown in Fig. 1(d). The scattering patterns originating from the magnetic maze domains are nearly symmetric azimuthally. There exists a small nonsystematic asymmetry in the measured patterns, that becomes less pronounced as the number of averaged frames is increased. In what follows this asymmetry is not taken into account being canceled out by azimuthal averaging to obtain the dependence of intensity I on scattering vector q (Fig. 1(e)). As seen from Figs. 1(d) and 1(e), the main effects of the IR pumping are a decrease of the scattering intensity in the low $q = 0.1\,\mathrm{nm}^{-1}$ region corresponding to the third-order scattering ring and the appearance of additional scattering at high $q > 0.2\,\mathrm{nm}^{-1}$ region. Full scattering maps I (q, dt,n) for the first $n = 1 - 10$ pulses in a train are given in Fig. 2(a). To remove the nonmagnetic charge scattering background, we calculate the difference signal $\Delta I(q,\ \Delta t, n) = I(q, \Delta t, n) - \langle I(q, n = 1)\rangle_{\Delta t<0}$ relative to the unpumped state present at the very beginning of the train. To quantify the degree of demagnetization, we further introduce $\Delta I_N(q,\ \Delta t, n) = \frac{\Delta I(q,\Delta t,n)}{\langle \Delta I(q=0.1\mathrm{nm}^{-1}, n=20)\rangle}$, i.e., a normalization (N = normalized) of the signal to the intensity observed at the end of the train, where a complete demagnetization is achieved Fig. 2(c). Such a normalization brings the intensity of the third-order scattering ring at $q = 0.1\,\mathrm{nm}^{-1}$ to a convenient range between 0 (100% magnetic contrast, i.e., unpumped) and −1 (zero magnetic contrast, i.e., total demagnetization). The time

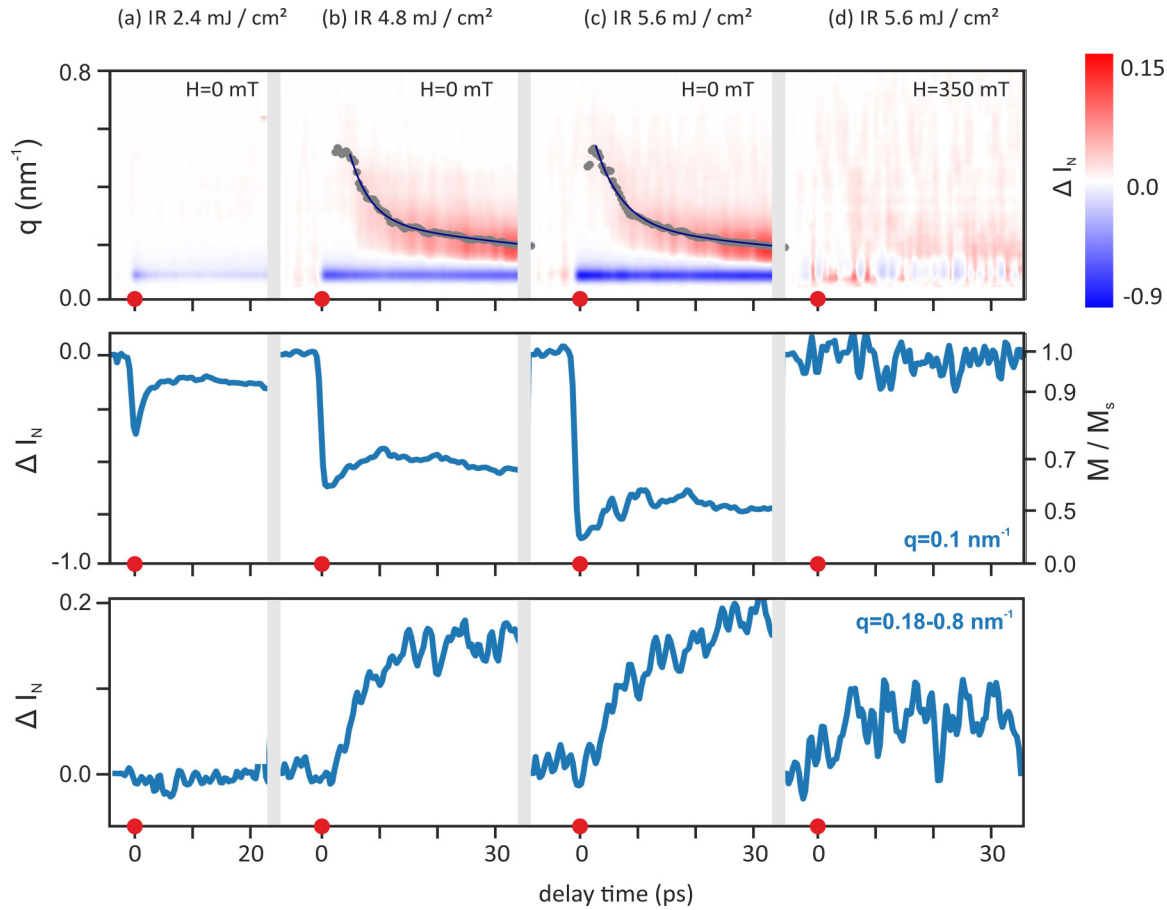

FIG. 3. Dependence of scattering intensity on fluence and out-of-plane magnetic field. Temporal evolution of difference intensity vs scattering vector $\Delta I_N(q,\ \Delta t)$ for (a)–(c) different IR fluences and (d) a magnetic field of 350 mT ($n = 1$, top row). In (b) and (c) the q position of maximum scattering intensity $q_{\max} = \max\{\Delta I_N(q)\}$ vs delay time Δt behavior (gray points) is fitted by a double exponential decay (solid blue line). The middle and bottom row show ΔI_N for $q = 0.1\ \text{nm}^{-1}$ and $q \in (0.18 - 0.8\ \text{nm}^{-1})$, respectively.

dependence of such normalized difference signal is presented in Fig. 2(b) showing blue colored regions of reduced low-q scattering at $\text{q} = 0.1\,\text{nm}^{-1}$ and red colored regions of the newly appeared high-q scattering at $\text{q} > 0.2\,\text{nm}^{-1}$. Within the first ten pumped pulses in a train ($n = 1-10$) both high-q and low-q magnetic scattering fade and eventually vanish indicating that thermal heating prevents the sample to recover to the initial state before the next pump pulse, cf. Figs. 2(a) and 2(b). The temporal evolution of the ΔI_N signal at $q = 0.1\ \ \text{nm}^{-1}$ corresponding to the third-order scattering from the magnetic maze-domain pattern [17] is shown in Fig. 2(c). Starting at $n = 1$, the third-order scattering signal significantly decreases upon IR-pumping on a subpicosecond timescale to a minimum value of $(\Delta I_N)_{\min}(q = 0.1\ \text{nm}^{-1}) = -0.8$ reflecting the process of ultrafast optical demagnetization (maximum reduction of saturation magnetization M down to $(\frac{M}{M_S})_{\min} = \sqrt{(\Delta I_N)_{\min} + 1} = 0.44$. Subsequently, during the maximum time delay of $\Delta t = +40$ ps and till the arrival of the second pump pulse in a train ($n = 3$) (i.e., 3.6 μs after the first IR-pulse), remagnetization occurs to about $(\Delta I_N)_{\text{remag}}(q = 0.1\ \text{nm}^{-1}) = -0.5$ or $(\frac{M}{M_S})_{\text{remag}} = 0.7$ in terms of magnetization. Hence, thermalization with the environment is not completed when the second pump pulse in a train arrives. Consequently, for each subsequent IR pulse, the minimum value of scattered intensity (magnetization) gradually gets smaller and the corresponding remagnetization is reduced. Eventually, the sample becomes completely demagnetized, i.e., enters the paramagnetic phase, after the fifth IR-pulse ($n = 9$).

In Fig. 2(d) the temporal evolution of the transient high-q scattering signal is given by integrating $\Delta I_N\ (q,\ \Delta t, n)$ in the q range of 0.18–$0.8\,\text{nm}^{-1}$. Starting at $n = 1$ the integrated intensity shows an increase for $\Delta t = 0-40$ ps. The high-q signal completely vanishes after 1.8 μs before the next IR-pump pulse. Eventually, for $n \geqslant 7$ no high-q scattering intensity occurs on picosecond time scales within the experimental statistics [see also Fig. 2(b) for $q \geqslant 0.2\ \text{nm}^{-1}$]. This particularly implies that the high-q scattering is absent for the paramagnetic phase that is reached for $n = 9$ as outlined above [Fig. 2(c)].

The fluence dependence of the difference scattering intensity $\Delta I_N(q,\ \Delta t, n = 1)$ is presented in Figs. 3(a)–3(c). Remarkably, both the low-q signal (reflecting the strength of demagnetization) and the transient high-q signal increase with IR fluence. For the lowest fluence of $f = 2.4$ mJ/cm², the transient high-q scattering signal is below the experimental resolution. To check, if the magnetic domain pattern is a necessary prerequisite for the high-q-scattering signal, we

have performed the pump-probe experiment in the single-domain state achieved by applying a perpendicular magnetic field of 350 mT. Remarkably, in addition to vanishing of the low-q scattering from the magnetic maze-domain pattern, also the transient high-q signal becomes strongly suppressed [Fig. 3(d)]. A quantitative measure for the effective length scale related to the high-q scattering signal is the q-position of the local maximum in the scattering intensity $q_{\max} = \max\{\Delta I_N(q)\}$. The temporal evolution of $q_{\max}$ is plotted in Figs. 3(b) and 3(c) with gray data points. A double exponential decay (blue line) with fluence-independent time constants of 5.0 ± 0.5 ps and 58 ± 4 ps reproduces the $q_{\max}(\Delta t)$ behavior quite well.

To relate the high-q transient scattering to the appearance of short-range magnetic fluctuations during the ultrafast demagnetization of the magnetic maze domains, we deployed an atomistic spin model based on the two-temperature approach describing the behavior of the magnetic maze domain pattern upon ultrafast IR pumping [1]. Usually, the multidomain state in multilayer magnetic systems [6,17,18] is explained by the competition between the nearest-neighbor ferromagnetic exchange interaction and the long-range anisotropic dipole-dipole interaction [17,19]. Since the nearest-neighbor interaction, favoring a collinear orientation of spins is much stronger than the dipole-dipole interaction, the resulting domain structures exhibit a rather long periodicity. But the long-range character of the dipole-dipole interaction complicates theoretical modeling, since coupling between magnetic moments located far apart cannot be neglected and a summation over the whole lattice is required.

The other microscopic mechanism that can reproduce multidomain patterns of labyrinth type (spin spirals) in metallic magnets [20,21] is based on the competing ferromagnetic exchange and Dzyaloshinskii-Moriya interactions (DMI) [22,23]. In contrast to dipole-dipole interaction discussed above, DMI is short-range and favors an orthogonal configuration of the neighboring spins. In the case of multilayer structures, the interfacial DMI can take place due to the symmetry breaking at the interfaces between magnetic and heavy metal layers [24]. Importantly, recent experiments on symmetric Pt/Co/Pt multilayers reported in Ref. [25] have demonstrated a stabilization of the room-temperature skyrmions at finite magnetic fields, which is a clear signature of the interfacial DMI in this system. Based on these experimental results we propose a magnetic model with Dzyaloshinskii-Moriya interaction for simulating long-range spin spiral structures in Co/Pt multilayers. We have used the following Hamiltonian:

$$H = -\sum_{i \neq j} J_{ij} \boldsymbol{S}_i \boldsymbol{S}_j - \sum_{i \neq j} \boldsymbol{D}_{ij} [\boldsymbol{S}_i \times \boldsymbol{S}_j] - K \sum_i \left(S_i^z\right)^2, \quad (1)$$

where $\boldsymbol{S}_i$ is the classical unit vector describing the direction of the corresponding spin, J_{ij} and $\boldsymbol{D}_{ij}$ are the isotropic exchange interaction and Dzyaloshinskii-Moriya vector, respectively. The last term in Eq. (1) corresponds to the single-ion anisotropy providing perpendicular alignment of magnetization within the domains. In our case this Hamiltonian is defined on a triangular lattice, mimicking the structure of single Co layer in Co/Pt [26]. The corresponding supercell of 500×500 is characterized by the periodic boundary conditions. For simplicity we drop the site indices, taking only nearest-neighbor couplings into account. The ratio of $\frac{|\boldsymbol{D}|}{J}$ controls the period of the spin spiral, which is defined as $\lambda = \frac{2\pi J a}{|\boldsymbol{D}|}$, where a is the nearest neighbor distance. Since the parameters of Eq. (1) corresponding to the Co/Pt multilayers are unknown, we fit them to reproduce the known experimental data. As was pointed out in Ref. [27], the Curie temperature of the material in question is below 500 K. On the other hand, one observes magnetic patterns of labyrinth type at room temperature. Taking into account these constrains we use $J = 1.5$ mRy. The chosen value of Dzyaloshinskii-Moriya interaction, $|\boldsymbol{D}| = 0.15$ mRy is enough to stabilize the spin spiral structures characterized by the pulse-driven scattering patterns in agreement with the experiment. The direction of Dzyaloshinskii-Moriya interaction vector for each pair of spins was set to be in-plane and lie perpendicular to the corresponding bond vector. The value of anisotropy constant, $K = 0.017$ mRy was taken from Ref. [13] obtained for similar multilayers as in our experiment.

Atomistic spin dynamics of the magnetic system was simulated by solving the Landau-Lifshitz-Gilbert (LLG) equation, as implemented in the Uppsala Atomistic Spin Dynamics (UppASD) package [28,29]:

$$\frac{d\boldsymbol{S}_i}{dt} = \frac{-\gamma}{1+\alpha^2} \boldsymbol{S}_i \times \left[\frac{-\partial H}{\partial \boldsymbol{S}_i} + \boldsymbol{b}_i(t) \right] - \frac{\gamma}{|\boldsymbol{S}_i|} \frac{\alpha}{1+\alpha^2} \boldsymbol{S}_i \times \left(\boldsymbol{S}_i \times \left[\frac{-\partial H}{\partial \boldsymbol{S}_i} + \boldsymbol{b}_i(t) \right] \right), \quad (2)$$

where γ is the gyromagnetic ratio, α is the Gilbert damping parameter and $\boldsymbol{b}_i(t)$ is the stochastic magnetic field. Gilbert damping controls the energy dissipation from the spin system and in our simulations, we set its value to $\alpha = 0.1$, which agrees with the previous estimates for similar systems [30]. The effect of the laser pulse on the magnetic structure was modeled with a two-temperature model in which the spin temperature T_s directly passes into LLG equation via the stochastic magnetic field b_i and is obtained from solving the two-temperature model [31]. The analytical expression for T_s is given by [32,33]:

$$T_s = T_0 + (T_P - T_0) \cdot \left(1 - e^{\frac{-t}{\tau_i}}\right) \cdot e^{\frac{-t}{\tau_f}} + (T_F - T_0) \cdot \left(1 - e^{\frac{-t}{\tau_f}}\right), \quad (3)$$

where T_0 is the initial temperature of the system, T_P is the peak temperature after the laser pulse is applied and T_F is the final temperature. The parameters τ_i and τ_f govern the time dependence of the spin temperature. In our simulations we have used $T_P = 750$ K, $T_0 = 300$ K, $T_F = 500$ K, $\tau_i = 0.22$ ps, $\tau_f = 5$ ps. The final temperature was chosen higher than the initial one to reflect the experimentally observed behavior of the system that was not able to fully cool down between the laser pulses. Using these parameters, one obtains the time evolution of the spin temperature shown in Fig. 4(f). Note that by employing such a simplified model, we neglect many physical mechanisms taking place after laser irradiation. Since the electron degrees of freedom are not considered, we cannot account, for instance, for optically induced spin transfer [34,35],

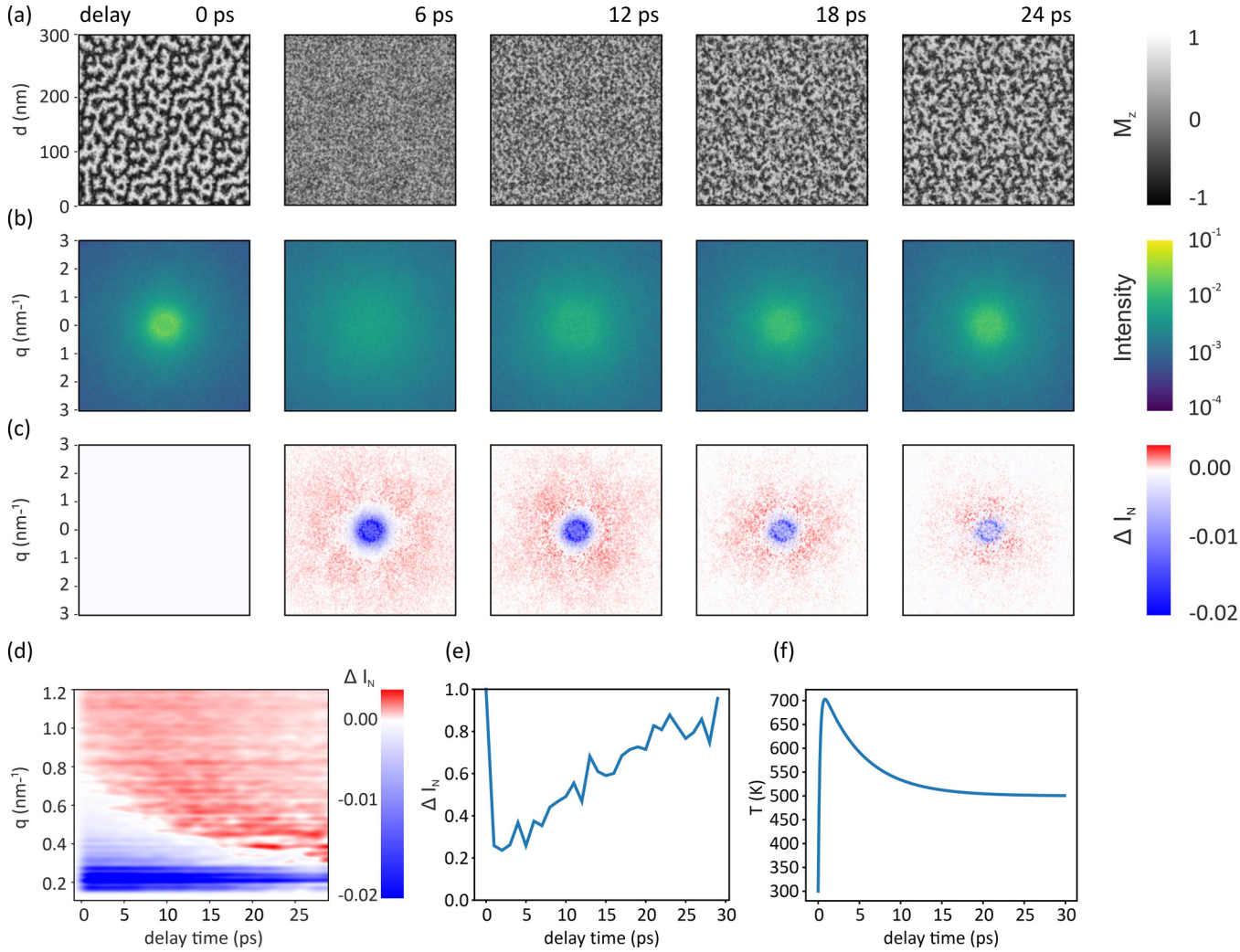

FIG. 4. Temporal evolution of the magnetic pattern and the corresponding scattering intensity upon laser excitation described by the two-temperature model. Evolution of the magnetic pattern (a), scattering intensity (b) and difference scattering intensity (c) within 30 ps after the laser pulse. Temporal evolution of the difference intensity vs scattering vector $\Delta I_N(q,\ \Delta t)$ (d). Intensity variation within the scattering ring corresponding to the initial domain structure (e). Time dependence of the spin temperature as obtained from LLG simulations within the two-temperature model (f).

which is usually active at times below 100 fs or superdiffusive spin transport [7,8], which induces additional torque acting on spins [36,37]. All these effects were neglected in the present analysis.

Simulations of the spin dynamics triggered by the laser pulse have revealed a partial destruction and reconstruction of the spin spiral structures in the system [Fig. 4(a)]. The closer view on the magnetization demonstrates the formation of small distorted spin spiral structures starting from 12 ps. As the temperature goes down, the small spirals coalesce to form new labyrinth structures in the system. To describe the magnetic scattering data, we have calculated the spin structure factor given by

$$\chi(\boldsymbol{q},t) = \frac{1}{N_{\text{spins}}}\left|\sum_i S_i^z(t)e^{-i\boldsymbol{q}\boldsymbol{r}_i}\right|^2, \tag{4}$$

where N_{spins} is the number of spins, $\boldsymbol{r}_i$ is the position of the ith atom. The scattering patterns obtained at different delay times are presented in Fig. 4(b). The patterns are almost azimuthally isotropic which is natural for a system with no anisotropy axis (e.g., crystallographic axis or magnetic field direction). Thus, when arbitrary oriented spin spirals are averaged across a sufficiently large area as it takes place in the mSAXS experiment, the resulting scattering pattern becomes isotropic. The slight pattern anisotropy present in Fig. 4(b) is explained by the relatively small grid used in the calculation. The difference scattering intensity $\Delta I(\boldsymbol{q},t) = \chi(\boldsymbol{q},t) - \chi(\boldsymbol{q},0)$ was as well calculated to highlight the transient changes of the scattering patterns [Fig. 4(c)]. At the time of the temperature peak, the high-q ring is mostly blurred under the influence of ultra-short-range thermal fluctuations, which seem to almost destroy the clear spiral structure in real space. This destruction is clearly seen as a negative (blue) ring at the low-q area of the scattering pattern. As the spin temperature goes down, the high-q (red) ring relaxes, gradually closing onto the low-q ring corresponding to the enlargement of the magnetic fluctuation. At the same time, the blue ring gets less intensive

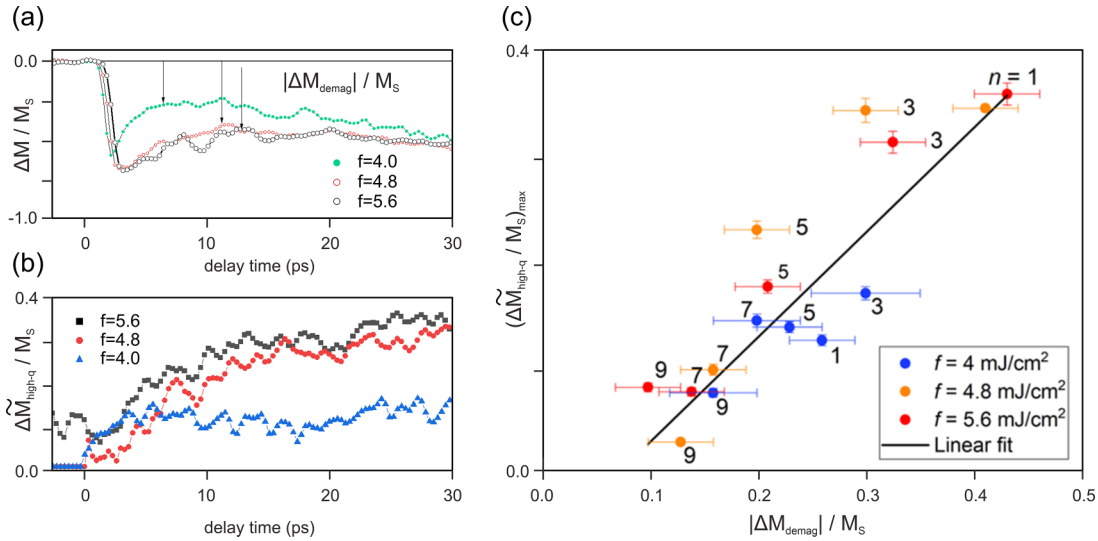

FIG. 5. Correlation between transient high-q scattering and demagnetization. Relative magnetization $\frac{\Delta M}{M_S}(q = 0.1\text{nm}^{-1},\ n)$ (a) and the integrated high-q signal $\frac{\Delta \tilde{M}_{\text{high-q}}}{M_S}(n) = \sqrt{\int_{0.15\ nm^{-1}}^{0.8\ nm^{-1}} \Delta I_N(q)\text{d}q}$ (b) as a function of delay time, for a fluence of $f = 4,\ 4.8,\ 5.6$ mJ/cm² and the first pumped pulse in a train. The strength of demagnetization per pump pulse $\frac{\Delta M_{\text{demag}}}{M_S}(n) = \frac{\Delta M}{M_S}(q = 0.1\text{nm}^{-1},\ \Delta t = 20\text{ ps}, n, f) - \frac{\Delta M}{M_S}(q = 0.1\text{nm}^{-1},\ \Delta t < 0\text{ ps}, n)$ is labeled in panel (a). (c) Transient magnetic signal $\frac{\Delta \tilde{M}_{\text{high-q,max}}}{M_S}$ as a function of strength of demagnetization $\frac{\Delta M_{\text{demag}}}{M_S}$ for different pulses in a train ($n \leqslant 9$) and fluences of $f = 4,\ 4.8,$ and 5.6 mJ/cm². The solid line is a linear fit to the data.

corresponding to gradual recovery of initial maze-domain order [Fig. 4(e)]. The time evolution of the corresponding radial $\Delta I(q)$ profiles is presented in Fig. 4(d) showing a qualitative agreement with experiment (compare to Fig. 3). Despite the simplicity of the considered spin Hamiltonian (which contains just isotropic and anisotropic exchange interactions between the nearest neighbors), the resulting spin dynamics of such a model subjected to the external pulse is rather nontrivial. In other words, the influence of the model parameters (such as magnetic coupling, damping factor, pulse structure and temperature) on the evolution of the high-q scattering rings is nonlinear and cannot be driven by a single parameter. This prevents us from one-to-one straightforward fitting of the theory to experiment. Nevertheless, our theoretical model reproduces all the main features and trends of the experiment and provides a microscopic explanation of the transient change of scattering patterns on the level of individual magnetic moments. Based on the results of these simulations, we can conclude that the reason behind the high-q scattering is that the laser pulse induces a thermal blurring of the initial spin-spiral magnetic structure that relaxes to a new spin-spiral state as the spin temperature decreases. To confirm the leading role of DMI in explaining the observed magnetic scattering behavior, one should examine the difference between scattering of left and right circular polarized light as described in Refs. [38,39]. We believe that this would be an interesting topic of future investigations.

IV. DISCUSSION

The obtained results unambiguously show that the presence of a magnetic domain pattern strongly enhances the high-q scattering signal. Since magnetic scattering is proportional to M_S^2 (as shown in Ref. [40]), in the following comprehensive analysis we deal with magnetization, namely $\frac{M_{\text{demag}}}{M_S}(\Delta t, n, f) = \sqrt{\Delta I_N(q = 0.1\ \text{nm}^{-1},\ \Delta t, n) + 1}$ and $\frac{\tilde{M}_{\text{high-q}}}{M_S}(\Delta t, n) = \sqrt{\Delta I_{N,\text{high }q}(\Delta t, n) + 1}$, in order to check for a correlation between strength of demagnetization and strength of high-q scattering signal. The strength of demagnetization triggered by the pump pulse is represented by the corresponding drop of $\frac{M_{\text{demag}}}{M_S}(\Delta t, n, f)$ over time delay, see Fig. 5(a). As a measure for the strength of the transient magnetization related to the high q-signal, we determined $\frac{\Delta \tilde{M}_{\text{high-q}}}{M_S}(n) = \sqrt{\int_{0.15\ nm^{-1}}^{0.8\ nm^{-1}} \Delta I_N(q)\text{d}q}$, see Fig. 5(b). The $\frac{M_{\text{demag}}}{M_S}$ vs $\frac{\tilde{M}_{\text{high-q}}}{M_S}$ dependence is shown in Fig. 5(c) for different pump pulses in a train ($n \leqslant 9$) and fluences of $f = 4,\ 4.8,$ and 5.6 mJ/cm², where the transient signal is strong enough to be clearly detected. Obviously, a linear relation between $\frac{\tilde{M}_{\text{high-q}}}{M_S}(n)$ and $\frac{M_{\text{demag}}}{M_S}(n)$ exists with a proportionality factor of 1.5 ± 0.3. Hence, the stronger the quenching rate of the magnetization within the domains, the stronger is the transient high-q magnetic signal corresponding to collective excitations. Since the scattering intensity at a wave vector q increases with the number of scatterers N according to $I \propto \sqrt{M} \propto N^2 \propto q^{-4}$ [41], $\frac{\tilde{M}_{\text{high-q}}}{M_S} > \frac{M_{\text{demag}}}{M_S}$ does not imply an increase of the global saturation magnetization. More importantly, the absolute decrease in the scattering intensity of the first order scattering peak is orders of magnitude stronger than the increase of $\frac{\tilde{M}_{\text{high-q}}}{M_S}(n)$ revealing that the nanoscale fluctuations are only minor perturbations compared to the overall demagnetization. Since the first-order scattering peak of the magnetic domains is not detected, a quantitative estimation of the absolute fluctuation strength is not possible at this point.

V. CONCLUSION

In conclusion, we report observation of short-range, transient magnetic fluctuations occurring at the 10-nm length scale upon ultrafast demagnetization in a maze-domain ferromagnetic Co/Pt multilayer system with perpendicular magnetic anisotropy. These fluctuations have been discovered by means of mSAXS in the wave vector region of 0.2–0.8 nm^{-1} at picosecond time scale. The transient signal appears in the ferromagnetic state only vanishing once the system is triggered beyond the ferromagnetic-paramagnetic phase transition and is strongly suppressed when the system is magnetized to saturation. Based on the detailed investigation of the transient signal as a function of IR-fluence and applied magnetic field, we reveal that the observed behavior has a purely magnetic nature and is related to the short-range fluctuations of the magnetic domain pattern upon optical excitation. A direct correlation between demagnetization strength and the intensity of a variable radius high-q transient scattering accompanying the nucleation of the short nanometer range magnetic fluctuations is found. This correlation allows to draw a conclusion that the demagnetization occurs not solely through domain wall broadening, as was earlier suggested by Pfau *et al.* [6], but in a more complicated way: through appearance of nanometer-range magnetic fluctuations. The low-q scattering from the domain structure coexists with the high-q scattering from the magnetic fluctuations for tens of picoseconds after the pumping event. Most reasonably the short-range fluctuations nucleate at the domain boundaries where the inhomogeneity of the magnetization distribution exists initially. Once the temperature of the spin system goes down after the IR pulse, a coalescence of the optically induced magnetic fluctuations takes place while corresponding magnetic scattering shifts gradually to the lower q values. The presented two-temperature atomistic spin model describes qualitatively the behavior of an optically pumped spin system at the 100 ps time scale. A temporal behavior of the correlations appearing in the magnetization ensemble is predicted by the model and compared to the experimentally observed time-resolved magnetic small-angle scattering patterns. Based on the simulation results, we interpret the high-q scattering as the result of the laser-driven heating inducing thermal fluctuations of the domain magnetic structure. The value of the presented study is related to the unraveling of the ultrafast magnetic response upon optical pumping. The obtained knowledge is indispensable for the development of potential ultrafast spintronic applications and from the point of the fundamental physics involved. The results contribute to the creation of an effective tool for controlling laser-excited spins in microscopically engineered magnetic materials. The study of dynamics of nanoscale inhomogeneities is of general importance for many fundamental phenomena, such as crystal growth, the role of fluctuations in high-T superconductors, and the emergence of quantum electronic phases hidden in thermal equilibrium.

All data are available in the main text or the Supplemental Material. Additional data related to this paper may be requested from the authors (S.M.S).

ACKNOWLEDGMENTS

The XFEL experiment has been carried out along proposal 2313. We acknowledge financial support from the VEKMAG end-station by the German Federal Ministry for Education and Research (BMBF 05K10PC2, 05K10WR1, 05K10KE1) and by HZB. We acknowledge funding from the following institutions: the Ministry of Science and Higher Education of the Russian Federation (Agreement No. 075-15-2021-1349) (S.M.S., M.V.B.), the Swedish Research Council (V.R.) Project No. 2019–03569 (Y.O.K.), the Russian Science Foundation, Grant No. 21-72-10136 (A.Y.D., V.V.M.), and CNRS-MOMENTUM (E.J.).

S.M.S., M.V.B., E.Y.L., I.I.P., A.P.K., D.V.P., W.R., A.S., Leonard M., G.M., L.L.G., R.G., A.Y., M.T., J.S., B.V.K., G.G., R.C., Laurent M. performed the experiments at XFEL. A.Y.D. and V.V.M. performed the atomistic modelling with support from Y.O.K., A.I.L. and S.M.S. M.R. fabricated the samples and performed magnetic characterization. S.M.S. and A.P.K. interpreted the results. S.M.S., E.Yu.L., M.V.B. and D.V.P. analyzed SAXS data. S.M.S., E.Yu.L. and A.P.K. prepared the figures. I.I.P., E.J. and S.L.M. conceived the study. S.M.S. and A.P.K. wrote the manuscript with input from A.S. and E.J. Supervision was by I.I.P., S.M.S. and A.P.K.. All the authors commented on the manuscript.

The authors declare that they have no competing interests.

[1] E. Beaurepaire, J.-C. Merle, A. Daunois, and J.-Y. Bigot, Ultrafast spin dynamics in ferromagnetic nickel, Phys. Rev. Lett. **76**, 4250 (1996).

[2] A. Kirilyuk, A. V. Kimel, and T. Rasing, Ultrafast optical manipulation of magnetic order, Rev. Mod. Phys. **82**, 2731 (2010).

[3] D. Sander, S. O. Valenzuela, D. Makarov, C. H. Marrows, E. E. Fullerton, P. Fischer, J. McCord, P. Vavassori, S. Mangin, P. Pirro *et al.*, The 2017 magnetism roadmap, J. Phys. D **50**, 363001 (2017).

[4] B. Wu, D. Zhu, Y. Acremann, T. A. Miller, A. M. Lindenberg, O. Hellwig, J. Stöhr, and A. Scherz, Observations of laser induced magnetization dynamics in Co/Pd multilayers with coherent x-ray scattering, Appl. Phys. Lett. **99**, 252505 (2011).

[5] C. E. Graves, A. H. Reid, T. Wang, B. Wu, S. De Jong, K. Vahaplar, I. Radu, D. P. Bernstein, M. Messerschmidt, L. Müller *et al.*, Nanoscale spin reversal by nonlocal angular momentum transfer following ultrafast laser excitation in ferrimagnetic GdFeCo, Nat. Mater. **12**, 293 (2013).

[6] B. Pfau, S. Schaffert, L. Müller, C. Gutt, A. Al-Shemmary, F. Büttner, R. Delaunay, S. Düsterer, S. Flewett, R. Frömter *et al.*, Ultrafast optical demagnetization manipulates nanoscale spin structure in domain walls, Nat. Commun. **3**, 1100 (2012).

[7] M. Battiato, K. Carva, and P. M. Oppeneer, Superdiffusive spin transport as a mechanism of ultrafast demagnetization, Phys. Rev. Lett. **105**, 027203 (2010).

[8] M. Battiato, K. Carva, and P. M. Oppeneer, Theory of laser-induced ultrafast superdiffusive spin transport in layered heterostructures, Phys. Rev. B **86**, 024404 (2012).

[9] E. Iacocca, T.-M. Liu, A. H. Reid, Z. Fu, S. Ruta, P. W. Granitzka, E. Jal, S. Bonetti, A. X. Gray, C. E. Graves *et al.*, Spin-current-mediated rapid magnon localisation and coalescence after ultrafast optical pumping of ferrimagnetic alloys, Nat. Commun. **10**, 1756 (2019).

[10] D. Zusin, E. Iacocca, L. Le Guyader, A. H. Reid, W. F. Schlotter, T.-M. Liu, D. J. Higley, G. Coslovich, S. F. Wandel, P. M. Tengdin *et al.*, Ultrafast perturbation of magnetic domains by optical pumping in a ferromagnetic multilayer, Phys. Rev. B **106**, 144422 (2022).

[11] M. Hennes, A. Merhe, X. Liu, D. Weder, C. von Korff Schmising, M. Schneider, C. M. Günther, B. Mahieu, G. Malinowski, M. Hehn *et al.*, Laser-induced ultrafast demagnetization and perpendicular magnetic anisotropy reduction in a $Co_{88}Tb_{12}$ thin film with stripe domains, Phys. Rev. B **102**, 174437 (2020).

[12] N. Zhou Hagström, R. Jangid, M. Madhavi, D. Turenne, J. A. Brock, E. S. Lamb, B. Stoychev, J. Schlappa, N. Gerasimova, B. Van Kuiken *et al.*, Symmetry-dependent ultrafast manipulation of nanoscale magnetic domains, Phys. Rev. B **106**, 224424 (2022).

[13] G. Winkler, A. Kobs, A. Chuvilin, D. Lott, A. Schreyer, and H. P. Oepen, On the variation of magnetic anisotropy in Co/Pt(111) on silicon oxide, J. Appl. Phys. **117**, 105306 (2015).

[14] N. Zhou Hagström, M. Schneider, N. Kerber, A. Yaroslavtsev, E. Burgos Parra, M. Beg, M. Lang, C. M. Günther, B. Seng, F. Kammerbauer *et al.*, Megahertz-rate ultrafast x-ray scattering and holographic imaging at the european XFEL, J. Synchrotron Radiat. **29**, 1454 (2022).

[15] T. Noll and F. Radu, *Proceedings of Mechanical Engineering Design of Synchrotron Radiation Equipment and Instrumentation Conference (MEDSI'16), (11–16 September 2016), Barcelona, Spain* (JACoW, Geneva, Switzerland, 2017), pp. 370–373.

[16] M. Porro, L. Andricek, S. Aschauer, A. Castoldi, M. Donato, J. Engelke, F. Erdinger, C. Fiorini, P. Fischer, H. Graafsma *et al.*, The MiniSDD-based 1-mpixel camera of the DSSC project for the european XFEL, IEEE Trans. Nucl. Sci. **68**, 1334 (2021).

[17] O. Hellwig, A. Berger, J. B. Kortright, and E. E. Fullerton, Domain structure and magnetization reversal of antiferromagnetically coupled perpendicular anisotropy films, J. Magn. Magn. Mater. **319**, 13 (2007).

[18] T. Wang, D. Zhu, B. Wu, C. Graves, S. Schaffert, T. Rander, L. Müller, B. Vodungbo, C. Baumier, D. P. Bernstein *et al.*, Femtosecond single-shot imaging of nanoscale ferromagnetic order in CoPd multilayers using resonant x-ray holography, Phys. Rev. Lett. **108**, 267403 (2012).

[19] J. J. Alonso and J. F. Fernández, Theoretical simulation of the anisotropic phases of antiferromagnetic thin films, Phys. Rev. B **74**, 184416 (2006).

[20] B. Lebech, J. Bernhard, and T. Freltoft, Magnetic structures of cubic FeGe studied by small-angle neutron scattering, J. Phys. Condens. Matter **1**, 6105 (1989).

[21] I. E. Dzyaloshinskii, Theory of helicoidal structures in antiferromagnets. I. Nonmetals, JETP 19, 960 (1964), https://api.semanticscholar.org/CorpusID:52202982.

[22] I. Dzyaloshinsky, A thermodynamic theory of "Weak" ferromagnetism of antiferromagnetics, J. Phys. Chem. Solids **4**, 241 (1958).

[23] T. Moriya, Anisotropic superexchange interaction and weak ferromagnetism, Phys. Rev. **120**, 91 (1960).

[24] C. Moreau-Luchaire, C. Moutafis, N. Reyren, J. Sampaio, C. A. F. Vaz, N. Van Horne, K. Bouzehouane, K. Garcia, C. Deranlot, P. Warnicke *et al.*, Additive interfacial chiral interaction in multilayers for stabilization of small individual skyrmions at room temperature, Nat. Nanotechnol. **11**, 444 (2016).

[25] M. He, T. Xu, Y. Gao, C. Hu, J. Cai, and Y. Zhang, Mixed-type skyrmions in symmetric Pt/Co/Pt multilayers at room temperature, Materials **15**, 8272 (2022).

[26] B. Zimmermann, G. Bihlmayer, M. Böttcher, M. Bouhassoune, S. Lounis, J. Sinova, S. Heinze, S. Blügel, and B. Dupé, Comparison of first-principles methods to extract magnetic parameters in ultrathin films: Co/Pt(111), Phys. Rev. B **99**, 214426 (2019).

[27] J. Kimling, A. Philippi-Kobs, J. Jacobsohn, H. P. Oepen, and D. G. Cahill, Thermal conductance of interfaces with amorphous SiO_2 measured by time-resolved magneto-optic kerr-effect thermometry, Phys. Rev. B **95**, 184305 (2017).

[28] B. Skubic, J. Hellsvik, L. Nordström, and O. Eriksson, A method for atomistic spin dynamics simulations: Implementation and examples, J. Phys. Condens. Matter **20**, 315203 (2008).

[29] O. Eriksson, A. Bergman, L. Bergqvist, and J. Hellsvik, *Atomistic Spin Dynamics: Foundations and Applications* (Oxford University Press, Oxford, 2017).

[30] A. Barman, S. Wang, O. Hellwig, A. Berger, E. E. Fullerton, and H. Schmidt, Ultrafast magnetization dynamics in high perpendicular anisotropy [Co/Pt]*n* multilayers, J. Appl. Phys. **101**, 09D102 (2007).

[31] U. Bovensiepen, Coherent and incoherent excitations of the Gd(0001) surface on ultrafast timescales, J. Phys. Condens. Matter **19**, 083201 (2007).

[32] J. H. Mentink, J. Hellsvik, D. V. Afanasiev, B. A. Ivanov, A. Kirilyuk, A. V. Kimel, O. Eriksson, M. I. Katsnelson, and T. Rasing, Ultrafast spin dynamics in multisublattice magnets, Phys. Rev. Lett. **108**, 057202 (2012).

[33] R. Chimata, L. Isaeva, K. Kádas, A. Bergman, B. Sanyal, J. H. Mentink, M. I. Katsnelson, T. Rasing, A. Kirilyuk, A. Kimel *et al.*, All-thermal switching of amorphous Gd-Fe alloys: Analysis of structural properties and magnetization dynamics, Phys. Rev. B **92**, 094411 (2015).

[34] J. K. Dewhurst, P. Elliott, S. Shallcross, E. K. U. Gross, and S. Sharma, Laser-induced intersite spin transfer, Nano Lett. **18**, 1842 (2018).

[35] F. Willems, C. von Korff Schmising, C. Strüber, D. Schick, D. W. Engel, J. K. Dewhurst, P. Elliott, S. Sharma, and S. Eisebitt, Optical inter-site spin transfer probed by energy and spin-resolved transient absorption spectroscopy, Nat. Commun. **11**, 871 (2020).

[36] P. Baláž, M. Žonda, K. Carva, P. Maldonado, and P. M. Oppeneer, Transport theory for femtosecond laser-induced spin-transfer torques, J. Phys. Condens. Matter **30**, 115801 (2018).

[37] P. Baláž, K. Carva, U. Ritzmann, P. Maldonado, and P. M. Oppeneer, Domain wall dynamics due to femtosecond laser-induced superdiffusive spin transport, Phys. Rev. B **101**, 174418 (2020).

[38] J.-Y. Chauleau, W. Legrand, N. Reyren, D. Maccariello, S. Collin, H. Popescu, K. Bouzehouane, V. Cros, N. Jaouen, and A. Fert, Chirality in magnetic multilayers probed by the symmetry and the amplitude of dichroism in x-ray resonant magnetic scattering, Phys. Rev. Lett. **120**, 037202 (2018).

[39] N. Kerber, D. Ksenzov, F. Freimuth, F. Capotondi, E. Pedersoli, I. Lopez-Quintas, B. Seng, J. Cramer, K. Litzius, D. Lacour *et al.*, Faster chiral versus collinear magnetic order recovery after optical excitation revealed by femtosecond XUV scattering, Nat. Commun. **11**, 6304 (2020).

[40] J. Stöhr and H. C. Siegmann, *Magnetism* (Springer, Berlin, 2006).

[41] O. Glatter, O. Kratky, and H. C. Kratky, *Small Angle X-Ray Scattering* (Academic, New York, 1982).